Global Biogeochemical Cycles

RESEARCH ARTICLE
10.1029/2025GB008937

Dynamic Sinking and Surface-Area Based Decay Modeling Reduce Estimates of Gelatinous Zooplankton-Mediated Carbon Export to the Deep Sea

Č. E. Perharič Bailey[1,2], M. Vodopivec[1], G. J. Herndl[3,4], T. Tinta[1], and M. Ličer[1,5]

[1]Marine Biology Station, National Institute of Biology, Ljubljana, Slovenia, [2]Jozef Stefan International Postgraduate School, Ljubljana, Slovenia, [3]Department of Functional and Evolutionary Ecology, Bio-Oceanography and Marine Biology Unit, University of Vienna, Vienna, Austria, [4]Department of Marine Microbiology and Biogeochemistry, Royal Netherlands Institute for Sea Research, Den Burg, The Netherlands, [5]Office for Meteorology, Hydrology and Oceanography, Slovenian Environment Agency, Ljubljana, Slovenia

Abstract Gelatinous zooplankton (GZ) have been proposed as a potentially important but largely overlooked contributor to the biological carbon pump. However, estimates of GZ-derived carbon transfer efficiency to the ocean floor reflect uncertainties in key parameters that govern carbon export, leading to contrasting interpretations of the role of GZ in the biological carbon pump. This study addresses key simplifications in previous models, that is, constant sinking speed and mass-depending decay, by introducing (a) vertical sinking dynamically coupled to GZ biomass loss due to microbial decay and (b) a novel surface-area-dependent formulation of GZ biomass degradation. Under these new assumptions, global GZ carbon exports and transfer efficiencies are recomputed, capturing processes not considered in earlier models. While global GZ export from the euphotic zone remains similar to previous estimates ($\sim 3.8\,\mathrm{Pg\,C\,y^{-1}}$), accounting for 39 % of the total global particulate organic carbon (POC) export, introducing a sinking speed coupled to GZ biomass reduces GZ POC export to the seafloor by 14 % (to $1.03\,\mathrm{Pg\,C\,y^{-1}}$). Adding the surface-area based decay reduces export to the seafloor by 43 % (to $0.68\,\mathrm{Pg\,C\,y^{-1}}$). These results indicate that while GZ remains a major contributor to carbon export from the euphotic zone, earlier models overestimated GZ contribution to deep-ocean carbon sequestration. Our modeling assumptions are generic and transferable to other types of sinking and decaying particles and can be leveraged to improve estimates of POC export, thus advancing the understanding of the mechanical aspects of the biological carbon pump.

Plain Language Summary Gelatinous zooplankton (GZ) or "jellyfish" may influence the biological carbon pump through sinking of their fecal pellets and carcasses (i.e., GZ-derived particulate organic carbon or GZ-POC) into the deep ocean. However, how much of GZ-POC reaches the deep ocean remains uncertain, due to differing estimates of global GZ biomass, assumed GZ-POC sinking speeds and microbial degradation rates. The present study links the sinking speed of GZ-POC to its diminishing mass via degradation and assumes that their decay depends on their surface area, not just their mass. This provides a more physically and biologically realistic description of the process, because (microbial) degradation primarily occurs on exposed surfaces and decay reduces particle size. Both effects slow down sinking and reduce the amount of deep ocean GZ-POC export. Under these new assumptions, the amount of GZ-POC export that reaches the seafloor is up to 43 % smaller than quantified by earlier models, though still a sizable portion (34 %) of total POC export. Our framework can be transferred to other types of particles to improve estimates of global POC export and advances the understanding of the biological carbon pump.

T. Tinta and M. Ličer contributed equally to this work.

Key Points:

- The model links gelatinous zooplankton (GZ) sinking speed to its mass, with decay dependent either on its mass or surface area
- In comparison with previous studies, variable sinking speed and new decay dependencies reduce GZ carbon export to the seafloor by up to 43%
- GZ may contribute 39% to the total global particulate organic carbon export out of the euphotic zone

Supporting Information:

Supporting Information may be found in the online version of this article.

Correspondence to:

Č. E. Perharič Bailey,
crtomir.perharic@nib.si

Citation:

Perharič Bailey, Č. E., Vodopivec, M., Herndl, G. J., Tinta, T., & Ličer, M. (2026). Dynamic sinking and surface-area based decay modeling reduce estimates of gelatinous zooplankton-mediated carbon export to the deep sea. *Global Biogeochemical Cycles*, *40*, e2025GB008937. https://doi.org/10.1029/2025GB008937

Received 17 OCT 2025
Accepted 2 MAR 2026

Author Contributions:

Conceptualization: G. J. Herndl, T. Tinta, M. Ličer
Data curation: Č. E. Perharič Bailey, M. Ličer
Funding acquisition: M. Vodopivec, T. Tinta, M. Ličer
Methodology: Č. E. Perharič Bailey, M. Vodopivec, T. Tinta, M. Ličer
Software: Č. E. Perharič Bailey, M. Ličer
Supervision: T. Tinta, M. Ličer
Validation: Č. E. Perharič Bailey
Visualization: Č. E. Perharič Bailey, M. Ličer

1. Introduction

The ocean exchanges approximately 100 Pg of CO_2 per year with the atmosphere, while photosynthesis fixes approximately 50 Pg of dissolved inorganic carbon into organic matter per year (Field et al., 1998; Le Quéré et al., 2018). Following a chain of diverse biochemical reactions, this primary production ends up in a plethora of carbon-containing compounds stored in the biomass of different organisms, including gelatinous zooplankton. A fraction $(5 - 12\,\mathrm{Pg\,C\,y^{-1}})$ of this organic carbon is exported into the ocean's interior as particulate organic matter either via sinking, down-welling of surface waters (rich in dissolved organic matter) or active vertical migration of organisms (Boyd et al., 2019; Henson et al., 2012; Herndl & Reinthaler, 2013; Iversen, 2023). Through these processes, collectively termed the biological carbon pump, carbon can remain sequestered from the

Writing – original draft: Č. E. Perharič Bailey, M. Vodopivec, T. Tinta, M. Ličer
Writing – review & editing: Č. E. Perharič Bailey, M. Vodopivec, G. J. Herndl, T. Tinta, M. Ličer

atmosphere for decades to centuries, depending on (biological) re-mineralization and circulation dynamics, affecting the global carbon cycle and ultimately, the global climate (Buesseler et al., 2020; Burd, 2024; Iversen, 2023; Stukel & Ducklow, 2017).

However, estimates of particulate organic carbon (POC) and dissolved organic carbon (DOC) supply appear insufficient to support the observed demands of deep-sea organisms (Burd et al., 2010), indicating that key processes and sources of organic matter sustaining microbial metabolism in the deep ocean remain to be identified. This mismatch suggests that either microbial metabolic rates are underestimated (Giering & Evans, 2022) and/or important sources and pathways of organic (and inorganic) matter are not accounted for (Herndl et al., 2023). These uncertainties limit the ability to mechanistically understand, model, and close the carbon budget of the biological carbon pump (Berzaghi et al., 2025).

It has been suggested that gelatinous zooplankton (GZ)—including Medusozoa (Cnidaria), Ctenophora, and pelagic tunicata (*Thaliacea*, Chordata)—which have been largely overlooked contributors to oceanic carbon cycling, may represent one of the missing components linking surface-derived production to deep-sea microbial carbon demand (Steinberg & Landry, 2017). Gelatinous zooplankton have likely been overlooked due to methodological challenges, including poor capture by sediment traps, destruction by nets owing to their fragility, and high spatial and temporal patchiness in their populations, all of which complicate quantitative assessments of their carbon flux (Lebrato et al., 2012; Tinta et al., 2021).

GZ inhabit a wide range of marine ecosystems, occasionally forming large blooms with high biomass. Global-scale analyses combining microscopy-based plankton imaging with molecular (eDNA) data from the Tara Oceans expeditions indicate that gelatinous zooplankton can account for up to ∼30 % of total plankton biovolume, corresponding to approximately 9% of plankton carbon (Lombard et al., 2024). At the global scale, published estimates of gelatinous zooplankton biomass span a wide range, from 0.1 Pg C to 3.1 Pg C (Bar-On et al., 2018; Lucas et al., 2014; Luo et al., 2020; Wright et al., 2021).

Once GZ die off, their carcasses face different fates. They can be (a) consumed or fragmented by predators and scavengers (Sweetman et al., 2014), (b) degraded by pelagic communities (macro- and micro-organism) (Fadeev et al., 2024; Tinta et al., 2020, 2023), (c) sink intact through the water column as "jelly falls" (Lebrato et al., 2011, 2013) and/or (d) be degraded by benthic communities once reaching the seafloor (Guy-Haim et al., 2020; Sweetman et al., 2014, 2016). The amount of GZ-derived organic matter that reaches certain ocean depths depends on several other factors, such as the initial biomass distribution of GZ, mortality rates, their specific density and biochemical composition. Biomass of different GZ species differs in molecular composition (e.g., proteins, lipids, carbohydrates, and structural compounds) and elemental stoichiometry, which governs microbial accessibility and enzymatic degradation, and thus controls microbial remineralization rates and community composition as diverse microbes are equipped with distinct metabolic machinery (Boyd & Trull, 2007; Johnson et al., 2020; Turner, 2015). There are several other factors to account for, such as the depth where GZ die off, the predation and fragmentation rates, sinking speed, ambient seawater temperature and water column structure, as well as the composition and functional capacity of the marine food web. All these factors determine the fate of GZ-carbon in the ocean, with many unknowns that need to be addressed to accurately incorporate GZ into the ocean carbon budgets (Tinta et al., 2021).

Modeling efforts have highlighted substantial uncertainty in quantifying the contribution of GZ to particulate organic carbon (POC) export and the biological carbon pump. Early approaches, where GZ were modeled independently of ecosystem dynamics, estimated that they contribute $3.9 - 5.8\,\mathrm{Pg\,C\,y^{-1}}$ to the secondary production in the epipelagic ocean (Luo et al., 2020), corresponding to 7.8 − 11.6 % of the global marine primary production (Field et al., 1998). Furthermore, GZ were found to represent 32 − 40 % of the total global POC export at 100 m (Luo et al., 2020), with high transfer efficiencies (T_{eff}, i.e., the fraction of biomass reaching the ocean floor) of up to 40 % to the seafloor (Lebrato et al., 2019), indicating that they could represent some of the most important contributors to carbon sequestration in the deep ocean. However, these estimates are based on a relatively small number of studies (Lebrato et al., 2019; Luo et al., 2020), which mostly considered a scenario in which GZ carcasses rapidly sink through the water column, while being subjected to degradation by different pelagic organisms (Lebrato et al., 2013, 2019). These studies based their models on limited available data on sinking speeds and microbial decay rates, which have led to substantial uncertainties in quantifying their actual role in carbon export and sequestration (Tinta et al., 2021).

More recent fully coupled ecosystem–biogeochemical models, where GZ are included as an additional functional group within plankton food webs and constrained by surface nutrients, chlorophyll, and trophic structure, however, consistently report lower GZ biomass and reduced or redistributed POC export. The first such attempt was made by Wright et al. (2021), who studied the addition of cnidarians. They discovered that such an addition increases total export production by $0.1\,\mathrm{Pg\,C\,y^{-1}}$, however, the value is still lower than that of uncoupled models (Luo et al., 2020). Later, the inclusion of a tunicate functional group was studied by Luo et al. (2022). This was followed by the addition of fast sinking tunicate groups (Clerc et al., 2023; Luo et al., 2024), which found that these can disturb the system in a way that leads to a decrease in POC export to the deep ocean. None of the above-mentioned studies, however, have represented the full diversity of gelatinous zooplankton together.

It is important to note that all of these models, uncoupled or coupled, used two important assumptions: firstly, that the sinking speed is constant throughout the sinking process, and secondly, that the rate of mass decay is proportional to the decaying particle mass. Both assumptions have their limitations and the goal of this paper is to reach beyond them and to quantify the consequences.

The assumption of constant speed disregards the varying balance between weight, buoyancy and drag forces acting on the sinking particle while it decays. In other words, diminishing mass continuously changes the forces on the sinking particle, leading to a change in its sinking speed. Therefore, any type of mass decay will lead to a change in sinking speed, which should be taken into account in any future attempt to model any type of sinking particles in the presence of decay.

Furthermore, previous GZ modeling studies assumed that the rate of mass decay depends solely on the mass itself—the larger the mass, the faster the decay. However, decay may depend at least partially on the surface area of the sinking particle, rather than its mass. The argument for this is as follows. The fate of POC in the ocean is largely governed by microbial degradation (Herndl & Reinthaler, 2013). The simplest modeling description of this process treats the detritus as a bulk state variable, applying a constant degradation rate per unit biomass, as implemented in many global models (Aumont et al., 2015; Kriest & Oschlies, 2015; Luo et al., 2020; Yool et al., 2013). In contrast, particle-resolved approaches model detritus as individual particles, often as spheres (Alcolombri et al., 2021; Nguyen et al., 2022), whose mass decreases continuously through remineralization, with rates depending on particle biomass and composition (Alcolombri et al., 2021; Nguyen et al., 2022; Omand et al., 2020). Microbes re-mineralize sinking detrital particles by degrading complex compounds with extracellular enzymes, acting on surfaces of the particles (Arnosti, 2011; Enke et al., 2018). Thus, the particle surface area may play a more important role in enhancing biomass-specific re-mineralization rates compared to conventional models, where re-mineralization rates are set to be dependent on mass (Anderson et al., 2023).

In this paper we formulate a model that links the particle's mass decay to its sinking speed, and we allow the rate of decay to be dependent either on particle's mass or on its surface area. This is done by deriving and solving two new models of GZ sinking, assuming all GZ have a spherical shape. As we later discuss, such an assumption leads to a conservative estimation of the difference that these models contribute to further understanding GZ's role in deep-sea POC export. We recompute this export out of the euphotic zone, twilight zone and to the global ocean floor using realistic, observation-based initial estimates of surface GZ biomass distributions. By allowing an interplay of sinking and decay processes, this approach represents a step toward a more conceptually appropriate framework for describing the fate of sinking organic particles beyond gelatinous zooplankton.

2. Models of Sinking and Decaying GZ

2.1. Mass-Dependent GZ Decay and Its Coupling to Sinking Speed

The previously proposed model for microbial decay of GZ (Lebrato et al., 2019) assumes that its rate of decay, $\mathrm{d}m/\mathrm{d}t$, of the particle mass m is directly proportional to the mass itself,

$$\frac{\mathrm{d}m}{\mathrm{d}t} = -km, \tag{1}$$

where k is an observed decay rate constant. Two temperature dependencies for k were inferred from observations (Lebrato et al., 2019): an exponential dependence

$$k_{\text{exp}} = 0.140\,\text{d}^{-1}\,\exp\left(0.145\,^{\circ}\text{C}^{-1}T(z)\right) \tag{2}$$

and a linear dependence

$$k_{\text{lin}} = 0.064\,^{\circ}\text{C}^{-1}\,\text{d}^{-1}T(z) + 0.02\,\text{d}^{-1}, \tag{3}$$

where T is the ocean temperature, z is depth (in meters) and d stands for 1 day. An exponential decay rate is expected from physiology, as many metabolic rates scale exponentially with temperature. In their study Luo et al. (2020) used the exponential decay rate constant k_{exp} from Lebrato et al. (2019) to estimate GZ carbon export to the global ocean. This work by Luo et al. (2020) serves as a control experiment, which is replicated using the model from this study under the same assumptions. The reproduction of the baseline results is done to ensure that the model works correctly under the same assumptions. Results with exponential solutions are shown here, while results following a linear decay rate k_{lin} are available in Figures S3–S6 of Supporting Information S1 of this paper.

In addition to the rate of change in biomass, carbon export estimation requires a model for the sinking speed. The simplest approach is to use a constant speed with values reported in Lebrato et al. (2013). While this is a reasonable approach in cold waters, where the decay is slow, it is less optimal in warmer moderate and tropical oceans, where rapid decay of the particle's mass and volume lead to a change in the net forces acting on the sinking particle. Hence, a sinking speed model, which captures this net-force-change, should be used. The force balance for a spherical decaying particle sinking in a fluid is

$$-\rho_{gz}V\frac{\text{d}w}{\text{d}t} = -\rho_{gz}Vg + \rho_{oc}Vg + \frac{1}{2}\rho_{oc}C_D\pi r^2 w^2, \tag{4}$$

where w denotes the vertical component of the sinking velocity, and the terms on the right hand side describe gravity, buoyancy and drag force on the particle. C_D is the drag coefficient, g is the gravitational acceleration, while ρ_{gz} and ρ_{oc} denote GZ and oceans densities, respectively. The volume of a GZ particle can be expressed as $V = m/\rho_{gz}$, while its radius is $r = \left(3m/4\pi\rho_{gz}\right)^{1/3}$, assuming a spherical shape. Here, m stands for the mass of a particle. Note that the spherical assumption is not always ideal, as GZ come in different shapes and sizes, which have been shown to impact GZ sinking rates (Lebrato et al., 2013). However, introducing other shapes would require experimental quantification of ρ_{gz}, r, C_D and particle rotation, which is irrelevant in the spherical case. Furthermore, contemporary uncertainties in other variables (e.g., initial sinking speed, microbial decay rates) are likely far greater than the spherical-body assumption. This is further discussed in Section 3.5.

Next, let's assume that the sinking particle reaches its terminal speed (where vertical acceleration becomes negligible $\text{d}w/\text{d}t \sim 0$) on a timescale much shorter than the decay timescale k^{-1}. The left hand side in Equation 4 can then be set to zero. This leads to

$$w(t) = \left[\frac{8g}{3C_D}\left(\frac{\rho_{gz}-\rho_{oc}}{\rho_{oc}}\right)\right]^{1/2}\left(\frac{3}{4\pi\rho_{gz}}\right)^{1/6} m^{1/6}(t) = \gamma m^{1/6}(t), \tag{5}$$

where the $V(m)$ and $r(m)$ dependencies mentioned above have been used and a constant parameter $\gamma = \left[\frac{8g}{3C_D}\left(\frac{\rho_{gz}-\rho_{oc}}{\rho_{oc}}\right)\right]^{1/2}\left(\frac{3}{4\pi\rho_{gz}}\right)^{1/6}$ was introduced for brevity. Note, that γ is a constant factor whose value is weakly constrained due to difficulties in measuring ρ_{gz}. Nevertheless, γ can easily be estimated from known initial sinking speed $w(0) = w_0$ and initial mass $m(0) = m_0$. Inserting w_0 and m_0 into Equation 5, $w(t) = \gamma m^{1/6}(t)$ leads to $w_0 = \gamma m_0^{1/6}$ and thus

$$\gamma = \frac{w_0}{m_0^{1/6}}. \tag{6}$$

Reinserting this expression of γ into Equation 5 leads to:

$$w(t) = w_0 \left(\frac{m(t)}{m_0}\right)^{1/6}. \tag{7}$$

In other words, the need to quantify parameters ρ_{gz} and C_D was sidestepped, by making use of initial conditions (mass and sinking speed), which have previously been reported (Lebrato et al., 2013; Luo et al., 2020). The full dynamics of microbial decay of GZ is therefore described by a coupled set of ordinary non-linear differential equations

$$\frac{\mathrm{d}}{\mathrm{d}t}\begin{bmatrix} z \\ m \end{bmatrix} = \begin{bmatrix} -w_0(m/m_0)^{1/6} \\ -km \end{bmatrix}, \tag{8}$$

where $k = k(T(z(t)))$. The minus sign in front of w_0 is reintroduced since the z-axis is pointing upwards and negative $\mathrm{d}z/\mathrm{d}t$ implies sinking. In essence, there exists a nonlinear positive feedback loop between mass m and sinking speed w. Mass decay causes slower sinking, which in turn retains the particle higher in the water column where the water is typically warmer, causing greater re-mineralization and thus a more efficient mass decay.

2.2. Surface Area-Dependent GZ Decay

It is, however, not obvious that mass decay should be proportional exclusively to the mass of the particle. Decay of GZ-derived organic matter is largely driven by microbes colonizing particle surfaces, suggesting that the decay of GZ-derived particles is proportional primarily to their surface area. This parallels the well-established dynamics of marine snow particles, where particle shape, surface area, and fragmentation strongly regulate microbial breakdown (Burd & Jackson, 2009). GZ carcasses and fecal pellets can be viewed as large, short-lived marine snow particles, subject to similar surface-mediated microbial processes. In the lowest order, the relationship between the mass decay rate and particle surface area S can be a simple proportionality:

$$\frac{\mathrm{d}m}{\mathrm{d}t} = -\lambda S. \tag{9}$$

Note that the decay rate constant λ is fundamentally different from k, measured in Lebrato et al. (2019): while k describes mass decay rate per unit mass, λ describes mass decay rate per unit surface area. Therefore, a unit rescaling of k is required before one can use observations of k from Lebrato et al. (2019) in estimates of λ:

$$\lambda = k\frac{m_0}{4\pi r_0^2}. \tag{10}$$

This rescaling not only ensures the correct units, but also makes sure that the initial rate of mass decay $\mathrm{d}m/\mathrm{d}t$ is equal to the observed value $-km_0$ in both cases, regardless of whether one describes the decay to be mass or surface area dependent. In other words, Equation 10 translates the measurements of GZ decay (Lebrato et al., 2019) from mass dependent k to surface dependent λ. After starting from the same (observed) initial value of decay rate, both decay rate constants (k and λ) and decay processes begin to differ as is derived below.

As in Section 2.1, a spherical approximation is assumed, hence the surface area can be expressed as a function of mass:

$$S = 4\pi r^2 = 4\pi\left(\frac{3m}{4\pi\rho_{gz}}\right)^{2/3} = 4\pi\left(\frac{mr_0^3}{m_0}\right)^{2/3}. \tag{11}$$

Equation 9 can then be rewritten to

Table 1
Summary of Implemented Modeling Setups With Respect to Sinking Speed and Mass Decay Type

Setup name	Sinking speed	Mass decay type	Model equations
CSMD (Constant Speed, Mass Dependent)	Constant	Mass dependent	$\frac{\mathrm{d}}{\mathrm{d}t}\begin{bmatrix} z \\ m \end{bmatrix} = \begin{bmatrix} -w_0 \\ -k(t)\,m \end{bmatrix}$
VSMD (Variable Speed, Mass Dependent)	Variable	Mass-dependent	$\frac{\mathrm{d}}{\mathrm{d}t}\begin{bmatrix} z \\ m \end{bmatrix} = \begin{bmatrix} -w_0(m/m_0)^{1/6} \\ -k(t)\,m \end{bmatrix}$
VSAD (Variable Speed, Area Dependent)	Variable	Surface area-dependent	$\frac{\mathrm{d}}{\mathrm{d}t}\begin{bmatrix} z \\ m \end{bmatrix} = \begin{bmatrix} -w_0(m/m_0)^{1/6} \\ -k(t)\,m^{2/3}m_0^{1/3} \end{bmatrix}$

$$\frac{\mathrm{d}m}{\mathrm{d}t} = -4\pi\lambda r_0^2\left(\frac{m}{m_0}\right)^{2/3}. \tag{12}$$

Expressing λ again in terms of k using Equation 10, yields

$$\frac{\mathrm{d}m}{\mathrm{d}t} = -k(t)m^{2/3}m_0^{1/3}. \tag{13}$$

Thus, the full set of dynamical equations is again a coupled set of ordinary differential equations

$$\frac{\mathrm{d}}{\mathrm{d}t}\begin{bmatrix} z \\ m \end{bmatrix} = \begin{bmatrix} -w_0(m/m_0)^{1/6} \\ -k(t)m^{2/3}m_0^{1/3} \end{bmatrix}. \tag{14}$$

Note that no changes were made to the sinking speed equation, as the form of the force balance Equation 4 remains unchanged by any choice of microbial decay. The surface area-dependent mass decay equation $\mathrm{d}m/\mathrm{d}t = -k\,m^{2/3}m_0^{1/3}$ however differs from its mass-dependent version $\mathrm{d}m/\mathrm{d}t = -k\,m = -k\,m^{2/3}m^{1/3}$. Since the initial mass m_0 is always larger or equal to m, one can intuitively expect that the surface area-dependent decay Equation 14 is always faster than the mass-dependent decay Equation 8 and will always result in a lower carbon export. A stricter formal proof of this claim is shown in Text S3 of Supporting Information S1. All modeling setups described in this section are summed up in Table 1.

Note, that Equation 14 no longer contains any terms dependent on particle size due to the unit rescaling in Equation 10. In other words, since the particle size has been expressed with its mass, the size itself no longer plays a direct role in its vertical mass transport and decay—not because size would be irrelevant, but because mass can serve as its proxy. This is a direct consequence of the spherical particle assumption and would not hold for a general particle shape (see Section 3.5). One can therefore apply biomass initial conditions and compute vertical carbon export using a single particle of appropriate mass, rather than an ensemble of many particles of different sizes. For a formal proof of this argument see Text S4 in Supporting Information S1. This subtle fact will greatly reduce the numerical cost of the computation of global carbon export.

Different setups generally lead to differing total global carbon export estimates. One of the relevant aggregate measures used in this study is the total global GZ POC export $\mathcal{M}_C(z)$ (in units Pg C y^{-1}) at depth z. This number is obtained as the area-weighted sum of the carbon fluxes ϕ_C (in units g C m^{-2} y^{-1}) at depth z over all ocean cell longitudes i and latitudes j:

$$\mathcal{M}_C(z) = \sum_{i,j}\phi_C(i,j,z)S(i,j), \tag{15}$$

Table 2
Initial Conditions for Sinking Speed and Exit Depths per Phylum's Carcasses (Mortality) and Fecal Pellets (Egestion), Taken From Luo et al. (2020)

Phylum	Particle type	$w_0\,[\mathrm{m\,d^{-1}}]$	Exit depth [m]
Cnidaria	Mortality	1,100	20
	Egestion	100	20
Ctenophora	Mortality	900	20
	Egestion	100	20
Chordata	Mortality	1,000	50
	Egestion	700	50

where $S(i,j)$ denotes the area of the cell with longitude i and latitude j and $\phi_C(i,j,z)$ denotes the value of carbon flux (in units $\mathrm{g\,C\,m^{-2}\,y^{-1}}$) at depth z at location (i,j), calculated within a particular modeling setup.

2.3. CarbonDrift Module and Relevant Ocean Data Sets

To solve equations corresponding to the modeling setups from Table 1 a new Lagrangian tracking `python` module `CarbonDrift` has been developed (available at https://doi.org/10.5281/zenodo.15387010), which is integrated into a well known open-source Lagrangian modeling environment `OpenDrift` (Dagestad et al., 2018). `CarbonDrift` was written to be a subclass of the `OceanDrift` object in `OpenDrift`, which tracks ocean fluid parcels by time integration of parcel locations in a precomputed 3D velocity field from a numerical ocean model. In this study velocity fields are obtained from a Copernicus global ocean current climatology product (E.U. Copernicus Marine Service (CMEMS), 2023, global-reanalysis-phy-001-030-monthly-climatology). `CarbonDrift` thus models the vertical dynamics either by the use of Equation 8 or Equation 14, while inheriting capabilities of horizontal advection from `OpenDrift`. In addition to velocity fields, `CarbonDrift` takes additional inputs of 3D temperature fields from the NOAA World Ocean Atlas 2018 (Boyer et al., 2018; Locarnini et al., 2018) and ETOPO bathymetry (NOAA National Centers for Environmental Information, 2022). In this work, all the fields are remapped to a 1° grid resolution using climate-data-operators CDO utility (Schulzweida, 2023).

In terms of advection, no relevant impact on the modeled total carbon export was found. The reason for this lies in the sinking dynamics, where the logic from 2D projectile motion can be applied. There, the maximum distance of a projectile scales with the time-of-flight. The latter is determined by the height and initial vertical velocity. Similarly, for a particle sinking in a fluid, its horizontal displacement is proportional to its sinking time, which is in turn inversely proportional to its initial sinking speed. Therefore, only the fecal pellets of Cnidaria and Ctenophora phyla with initial sinking speeds of $100\,\mathrm{m\,d^{-1}}$ (see Table 2) traverse horizontal distances larger than 50 km (not shown). However, these particles are also subject to faster decay (due to their longer residence in the warmer surface layer), therefore, their total flux contributions to the deep ocean are small. On the other hand, other GZ particles, sinking faster than $100\,\mathrm{m\,d^{-1}}$, generally traverse less than 10 km horizontally during sinking (not shown) and typically remain within the same ocean cell with the same ocean temperature. Therefore, in Section 3 only simulations in the absence of any horizontal advection with ocean currents are presented.

2.4. Initial Conditions

GZ carbon content estimates in the ocean surface layer are taken from Luo et al. (2020), where specific values were computed using a bioenergetics model

$$\frac{dB}{dt} = n[(AE \cdot I) - R - RL - E - \mathrm{Pr}] - M \tag{16}$$

for each of the ocean biomes. Here n is the number density, AE the assimilation efficiency, I is prey ingestion, R is respiration, RL loss due to reproduction, E exudation, Pr is predation and M is the mortality rate. The last term together with egestion rate

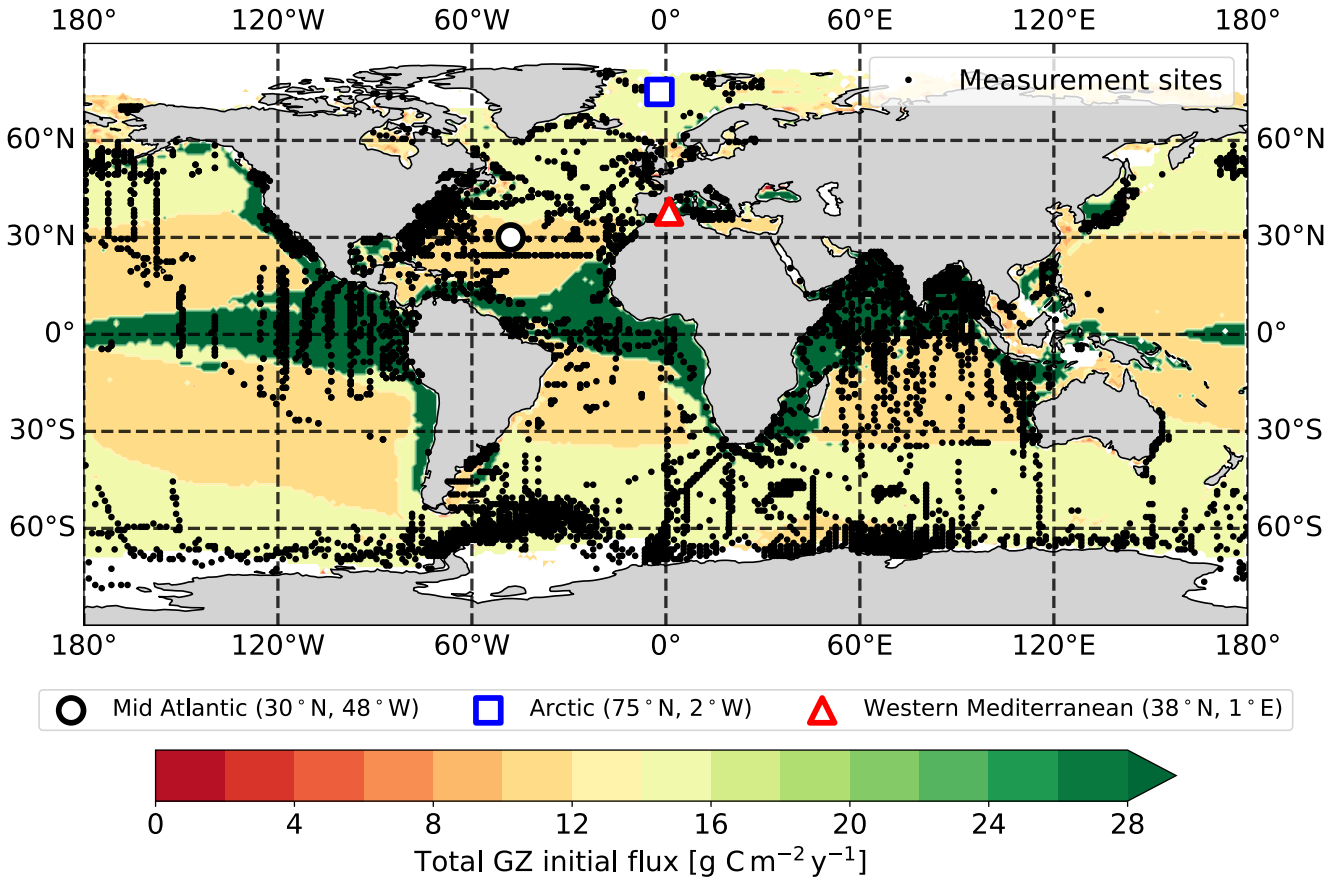

Figure 1. Colored regions depict the total initial GZ carbon flux, consistent with Luo et al. (2020), defined as the sum of mortality M and egestion E_g rates of the three major GZ phyla per unit area, calculated from observation-based estimates of GZ abundance and biomass measured at sites marked by black dots, as in Luo et al. (2020), mostly retrieved from the JeDI database (Condon et al., 2015; Lucas et al., 2014). White regions denote areas where insufficient data were available for biome construction. Three overlaid markers indicate selected sinking locations, where vertical sinking dynamics are explicitly studied in this paper.

$$Eg = n(1 - AE) \cdot I, \tag{17}$$

vertically integrated over the top 200 m, was computed as the export-available carbon content. Their mean baseline values (see Luo_M_Eg_biome_data.json in the supplementary data of https://doi.org/10.5281/zenodo.15387010) are used as initial POC export in this study as well.

The biomes in this study are defined following Luo et al. (2020), based on chlorophyll levels from NASA's SeaWiFS mission (NASA Ocean Biology Processing Group, 2025), maximum annual mixed layer depths (de Boyer Montégut, 2023; de Boyer Montégut et al., 2004) and ocean depth. Four biomes are thus constructed: (a) high-chlorophyll permanently stratified (HCPS), (b) high-chlorophyll seasonally stratified (HCSS), (c) low chlorophyll (LC) and (d) a coastal biome (COAST). Carbon content in each grid cell is calculated for each biome separately from in situ observations of GZ abundance and biomass (Figure 1, black dots) as in Luo et al. (2020). The observations are mostly retrieved from the JeDI database (Condon et al., 2015; Lucas et al., 2014). Available records of GZ occurrence, size, and wet weight are converted to carbon content using established conversion factors. The resulting initial carbon flux is distributed uniformly within each biome (see Text S1 of Supporting Information S1), such that biome-specific values inherently reflect features such as large coastal blooms present in the underlying observations.

Initial sinking speeds are simply the mean values used in Luo et al. (2020), and so are the exit depths of different phyla and their corresponding mortality and egestion rates (see Table 2). This close adherence to Luo et al. (2020)

is chosen to show that `CarbonDrift` can successfully reproduce results from Luo et al. (2020) by solving the system of Equation 8 with a constant sinking speed, corresponding to a CSMD setup in Table 1.

Variable sinking speed simulations, that is, time integration of systems Equations 8 and 14, are performed within `CarbonDrift` using the second order Runge-Kutta method, with a time step of 30 min and an output time-step of 1 h for initial vertical speeds $w_0 > 100\,\mathrm{m\,d^{-1}}$, or with an output timestep of 4 h for initial vertical speed $w_0 = 100\,\mathrm{m\,d^{-1}}$. The simulations are performed separately for each phylum and their corresponding mortality and egestion rates, which are then aggregated together during analysis.

3. Results and Discussion

Results presented in this paper are based on the initial GZ biomass estimates from Luo et al. (2020). The values of carbon export from their study serve as a control experiment, which have been reproduced independently using `Carbondrift` and their assumptions regarding constant sinking speed, initial biomass distribution (shown in Figure 1) and applying the same decay rates. These simulations, corresponding to the constant speed mass-dependent (CSMD) setup, result in the largest carbon export to the ocean floor since a particle's sinking speed is independent from its size and remains constant as it decays. Total global GZ POC export (sum of POC stored in fecal pellets and carcasses, in $\mathrm{Pg\,C\,y^{-1}}$) under this scenario amounts to $3.90\,\mathrm{Pg\,C\,y^{-1}}$ at 100 m, $1.84\,\mathrm{Pg\,C\,y^{-1}}$ at 1,000 m and $1.20\,\mathrm{Pg\,C\,y^{-1}}$ at the ocean floor. More information about these control simulations is available in the Text S2 and Table S1 of Supporting Information S1.

Section 3.1 contains comparisons of the CSMD setup with variable speed, mass-dependent (VSMD) and surface area-dependent (VSAD) setups. Incorporating variable sinking speed reduces total global GZ POC export to the ocean floor by 14 %, to $1.03\,\mathrm{Pg\,C\,y^{-1}}$. This is an expected effect of the non-linear coupling between sinking speed and mass: as the particle decays, its sinking speed drops, thus it is retained in warmer layers of the oceans longer, leading to a faster decay and, in turn, further deceleration. Adding surface area-dependent decay to the variable sinking speed setup increases the mass decay (Section 2.2). This reduces the total global GZ POC export to the ocean floor by 43 %, to $0.68\,\mathrm{Pg\,C\,y^{-1}}$.

Note that the values presented here are not associated with any uncertainty range. This is not because the uncertainty of these estimates would be zero, but rather, because the modeling additions in this study do not introduce any new uncertainties. They are simply carried over and appropriately scaled from Luo et al. (2020). The reductions following the new equations are exact, however, the uncertainties stemming from the initial export production distribution and measured sinking speeds stay the same. Further experimental work will likely reduce the uncertainties in export production and initial sinking speeds.

3.1. POC Flux Comparison Between Setups

The total global GZ-POC flux (in $\mathrm{g\,C\,m^{-2}\,y^{-1}}$) to different depths for the three modeling setups, that is, constant and variable sinking speed mass-dependent decay (CSMD and VSMD, respectively) and variable sinking speed surface area-dependent decay (VSAD) modeling setups is shown in Figure 2. As expected, in all setups the initial GZ POC export production determines the global GZ-POC export in the epipelagic ocean, corresponding to the largest POC export in the tropical regions of the Atlantic and Pacific, but also in the northern Indian ocean. In all setups, ocean temperatures lead to a rich spatial structure of GZ-POC export within each biome, even though the biome itself is initially populated with a constant spatial export production surface density. Meridional gradients in carbon export at each depth in Figure 2 therefore reflect meridional temperature gradients in the global ocean. In all modeling setups the largest flux reduction during the sinking process happens in the warm tropical oceans. Here, the flux is $7 - 19\,\mathrm{g\,C\,m^{-2}\,y^{-1}}$ at 100 m depth and $1 - 3\,\mathrm{g\,C\,m^{-2}\,y^{-1}}$ at the seafloor. In contrast, some regions in the polar and/or shallow water oceans retain much of their initial POC export down to the seafloor.

Explicit differences between constant and variable sinking speed and between mass and surface area-dependent decay rates are shown in Figure 3. When compared to the CSMD setup, the VSAD setup leads to lower POC fluxes than VSMD. At the depth of 100 m local fluxes are reduced up to $2.5\,\mathrm{g\,C\,m^{-2}\,y^{-1}}$ compared to CSMD, whereas in the deep ocean these differences can add up to $4\,\mathrm{g\,C\,m^{-2}\,y^{-1}}$. The largest differences occur at low latitudes, which is expected, since the difference scales with ocean temperature, as derived in the Text S3 of Supporting Information S1. This is further supported visually (Figure S9 of Supporting Information S1), by

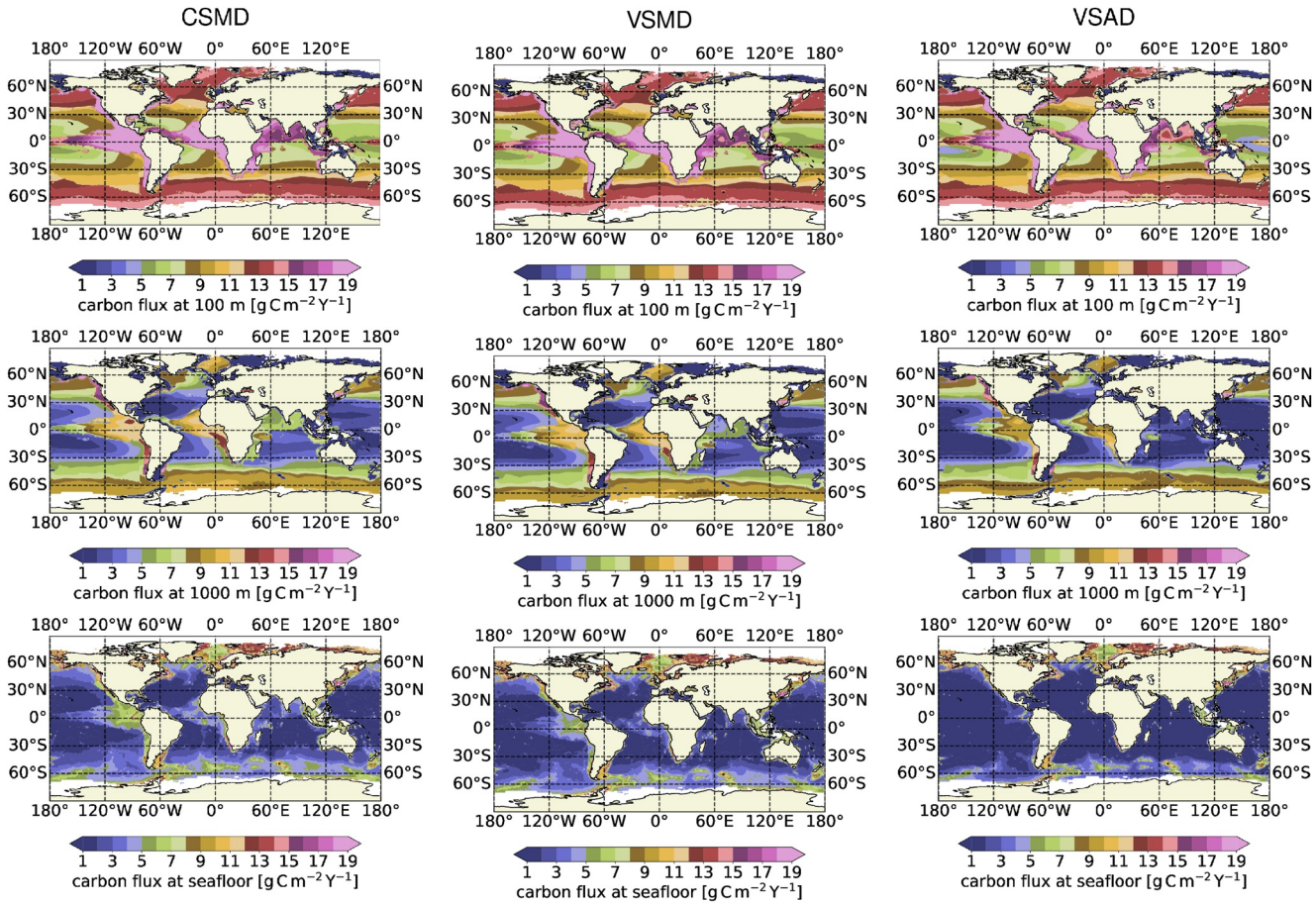

Figure 2. Total GZ POC flux at depths of 100 m (top row), 1,000 m (center row) and at the seafloor (bottom row) using an exponential decay rate. Left column: Mass-dependent decay model with a constant sinking speed (CSMD). Center column: Mass-dependent decay model with a variable sinking speed (VSMD). Right column: Surface area-dependent decay model with a variable sinking speed (VSAD).

computing the GZ POC flux difference between the VSMD and VSAD models. There, assuming a surface area-dependent decay, local fluxes to the seafloor are reduced up to 3 g C m^{-2} y^{-1} and roughly 1 g C m^{-2} y^{-1} at lower and temperate latitudes, respectively. For a comparison of zonal averages of GZ-POC fluxes between different model setups see Text S6 and Figure S2 in Supporting Information S1.

Variable sinking speed (VSMD setup) implies a reduction in sinking speed (in comparison to constant sinking speed setup) and hence in the POC flux. This effect is not apparent at the ocean surface but becomes more notable at greater depths in the tropical and temperate ocean, as shown in Figure 3. This is expected since sinking speeds decrease relatively slowly (on k^{-1} timescale) and this effect takes time to accumulate over the entire sinking process.

3.2. Vertical Profiles for a Variable Speed Mass-Dependent Decay Setup

The vertical profile of mass decay is determined by the initial sinking speed as seen in Figure 4. Here, the variable speed mass decay (VSMD) setup for all major phyla, Cnidaria, Chordata and Ctenophora, characterized by different sinking speeds of their carcasses (M) as well as of their fecal pellets (E_g) is shown. The plots are shown for the Mid-Atlantic, Arctic and Western Mediterranean locations. These locations were chosen because they exhibit a vast range of sinking dynamics due to varying vertical temperature profiles. As expected, all locations exhibit the fastest decay of egested particles (i.e., fecal matter production) from Ctenophora and Cnidaria, which have the lowest initial sinking speed and therefore spend more time in a warmer upper ocean. In the Mid-Atlantic and Western Mediterranean no egested mass remains below 500 m depth. In contrast, 15 – 25 % of other

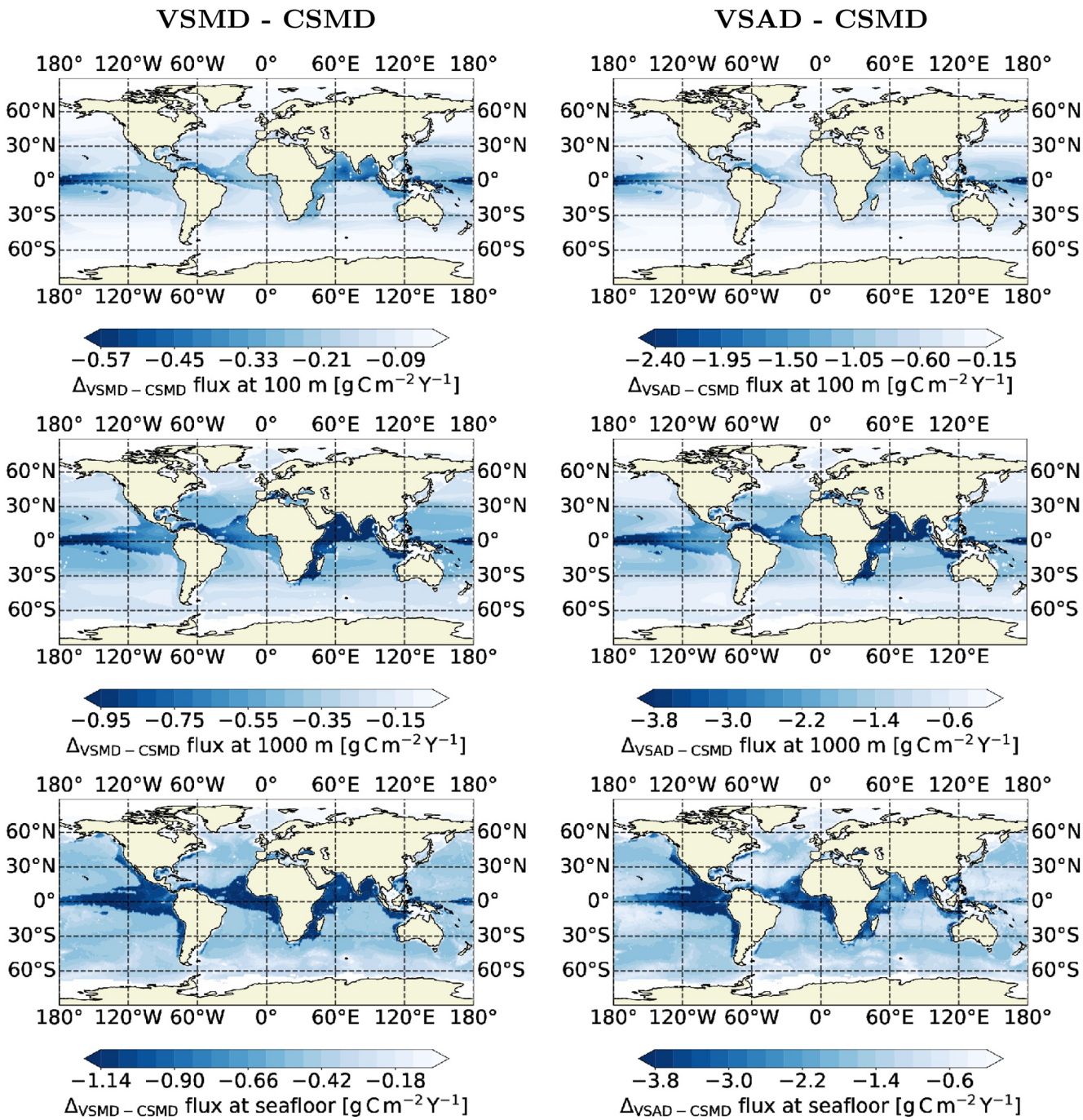

Figure 3. Total GZ POC flux difference between different model types at depths of 100 m (top row), 1,000 m (center row) and at the seafloor (bottom row) using an exponential decay rate. Left column: VSMD versus CSMD setup difference. Right column: VSAD versus CSMD difference. See Table 1 for setup definitions.

decaying particles reach the bathypelagic zone (below 1,000 m depth) in the Mid-Atlantic and 25 – 35 % of them reach the bathypelagic zone in the Western Mediterranean. In the Arctic ocean about 25 % of the egested mass and roughly 80 % of the total carcass mass reach the bathypelagic zone.

Constant sinking speed would produce straight lines in the plot of vertical trajectories (Figure 4). The effect of variable sinking speed is most pronounced for the slowest (egested) particles in a warmer Atlantic ocean, where the curve quickly flattens, that is, the particles reach a much shallower depth. The speed of sinking carcasses is, however, mildly reduced only after a substantial proportion of their entire sinking process (below 1,000 m depth).

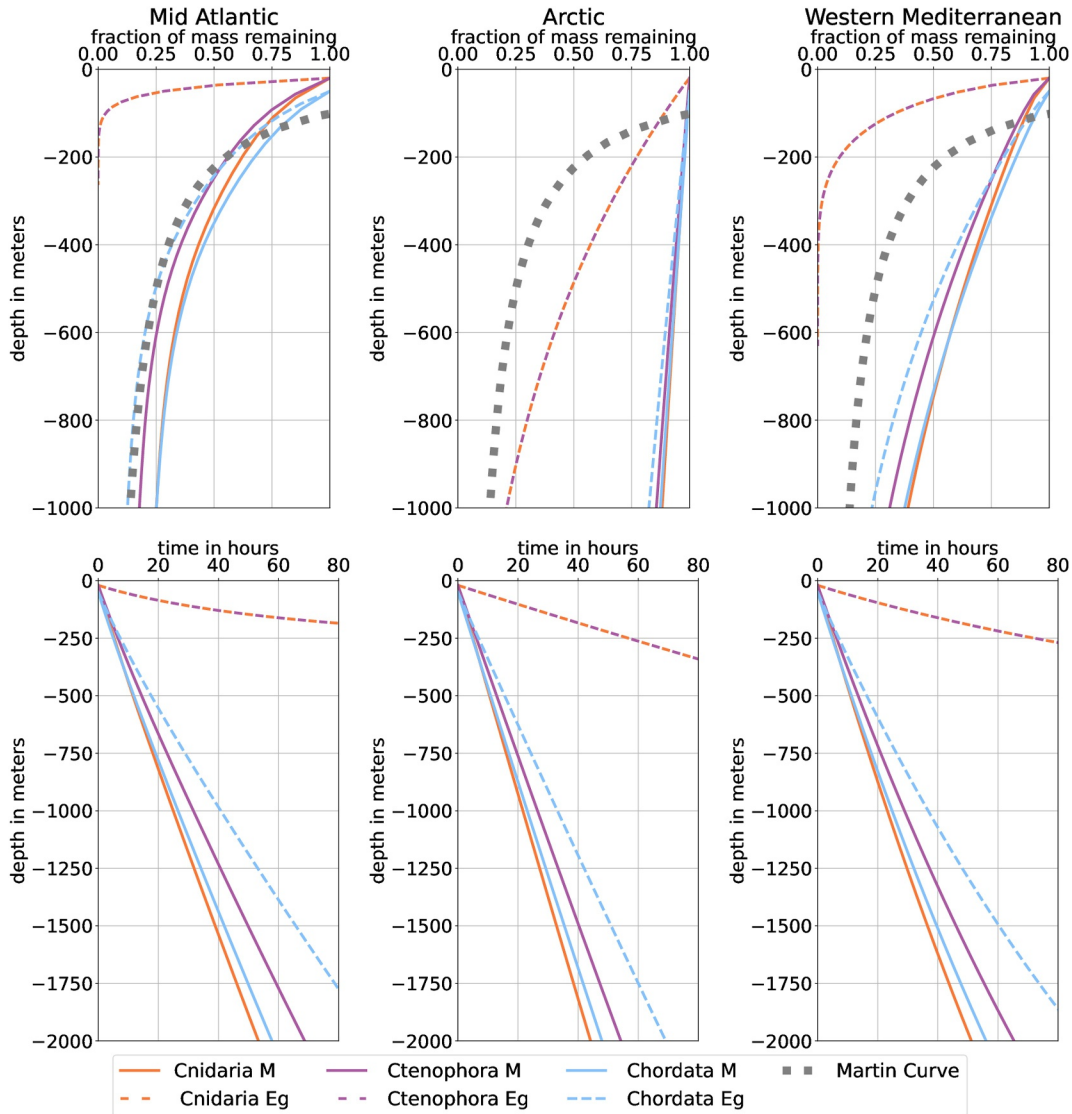

Figure 4. Fraction of mass attenuation with depth (top row) and vertical particle trajectories (bottom row) for particles with different initial vertical speeds at different locations (see Figure 1). Solutions for the mass-dependent—exponential decay rate with a variable sinking speed (VSMD) model are shown. Solid lines represent GZ carcasses (marked as mortality M), whereas dashed lines represent their fecal pellets (marked as egestion E_g). Orange lines represent the Cnidaria phylum, purple lines represent the Ctenophora phylum, whereas blue lines represent the Chordata phylum. Thick gray dotted lines show the Martin curve (Martin et al., 1987) with the slope parameter set to $b = 0.86$ and the reference (exit) depth $z_0 = 100$ m.

This effect is most notable for Ctenophora carcasses, since these have the lowest initial sinking speed of the three phyla (see Table 2). Note, however, that the sinking speed in the Arctic remains almost constant (the trajectories are almost straight lines) for all carcasses and egested particles due to low temperatures and a very slow decay. Global maps of final sinking speeds for both variable sinking speed models are available in the Text S7; Figures S7 and S8 of Supporting Information S1. Finally, note that relative mass and trajectories of egested particles from the Cnidaria and Ctenophora phyla are exactly the same. This is a reminder that vertical sinking speed depends only on the relative mass ratio and is thus the same for all organic particles with equal initial sinking speeds.

Comparing the sinking of a specific organic particle (Chordata fecal pellets) at the same specific locations between the three models (CSMD, VSMD and VSAD), leads to a similar conclusion as before. In a warmer ocean, clear differences arise in the trajectories and in the vertical profiles of the egested mass, whereas in the Arctic they are barely noticeable (see Text S5 and Figure S1 in Supporting Information S1).

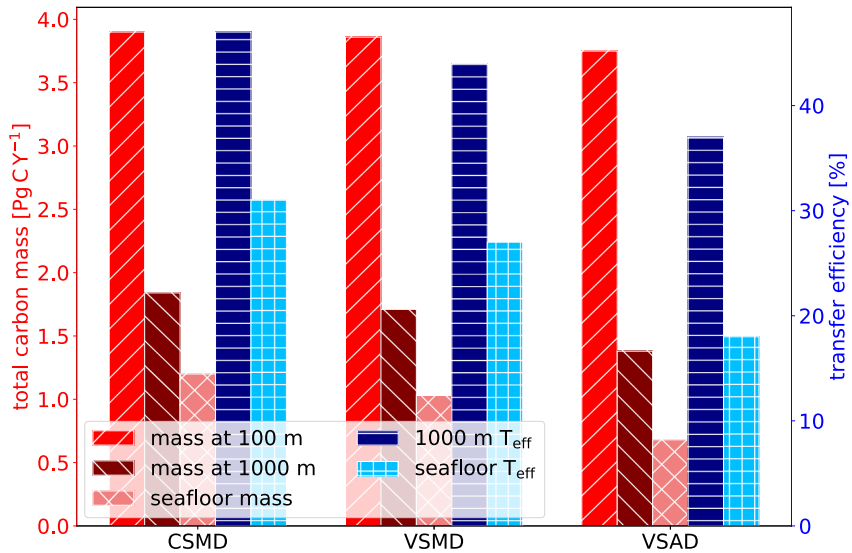

Figure 5. Left (red) axis: total global sum of carbon mass transport (red bars). Right (blue) axis: transfer efficiency T_{eff}, that is, the fraction of biomass reaching the ocean floor (blue bars) comparison between different models using an exponential decay rate.

3.3. Total Global Gelatinous Zooplankton POC Export

Total global GZ POC export $\mathcal{M}_C(z)$, defined by Equation 15, is computed for all setups at different depths z, and shown in Figure 5.

Recall that previous estimates, that is, from the constant sinking speed mass decay (CSMD) setup, were 3.90 Pg C y^{-1}, 1.84 Pg C y^{-1} and 1.20 Pg C y^{-1} at depths of 100, 1,000 m and at the seafloor, respectively. These values are clearly reduced in the variable sinking speed mass-dependent and surface area-dependent decay (VSMD and VSAD, respectively) setups (Figure 5). Within the VSMD setup, total GZ POC export at depths of 100, 1,000 m and at the seafloor is computed to be 3.86 Pg C y^{-1}, 1.71 Pg C y^{-1} and 1.03 Pg C y^{-1}, respectively. At the ocean floor, this amounts to a 14 % reduction with respect to the CSMD setup. For the VSAD model these values are 3.75 Pg C y^{-1} at 100 m, 1.38 Pg C y^{-1} at 1000 m and 0.68 Pg C y^{-1} at the seafloor. Combining surface area dependence of decay and variable sinking speed thus reduces total carbon export to the seafloor by 43 %.

As mentioned above, several attempts have been made to determine the role of GZ in the biological carbon pump using biogeochemical models with an explicit GZ component and CMSD. Focusing on the study of tunicata (Chordata) export by Clerc et al. (2023), they showed that 0.43 Pg C y^{-1}, 0.42 Pg C y^{-1} and 0.39 Pg C y^{-1} reach the depths of 100 m, 1000 m and the seafloor, respectively. This is much less than the CSMD control in this study, which resulted in 3.07 Pg C y^{-1}, 1.47 Pg C y^{-1} and 0.92 Pg C y^{-1}, respectively. The difference is mostly due to the altered modeling of GZ (biogeochemical model vs. static observations-based distribution) and the use of different initial sinking speeds for tunicata carcasses (800 m d^{-1} vs 1000 m d^{-1}) and their fecal pellets (1000 m d^{-1} vs 700 m d^{-1}). The VSAD model from this study leads to a reduced 2.98 Pg C y^{-1}, 1.09 Pg C y^{-1} and 0.49 Pg C y^{-1} compared to the CSMD control, respectively. These estimates are, however, still considerably higher compared to Clerc et al. (2023). Nevertheless, using the VSAD (or VSMD) setup in Clerc et al. (2023), would reduce their estimates even further. Other phylum specific POC export values at depth are available in Table S2 of Supporting Information S1.

The total global estimate of POC export based on currently quantified and known carbon sources to the depth of 100 m ranges from $5 - 12$ Pg C y^{-1} (Clements et al., 2023; DeVries & Weber, 2017; Henson et al., 2011; Nowicki et al., 2022; Siegel et al., 2014). Because the models in this study use the mean initial GZ export production estimates from Luo et al. (2020), their outputs should be compared to mean estimates of the total global POC export. Therefore, taking a mean value of 10 Pg C y^{-1} (Middelburg, 2019), GZ-POC export in the case of CSMD accounts for 39 % of the total global POC export. In the case of the VSMD model, the value is practically the same at 38.6 %, whereas in the VSAD model it is only slightly reduced to 37.5 %. However, at the

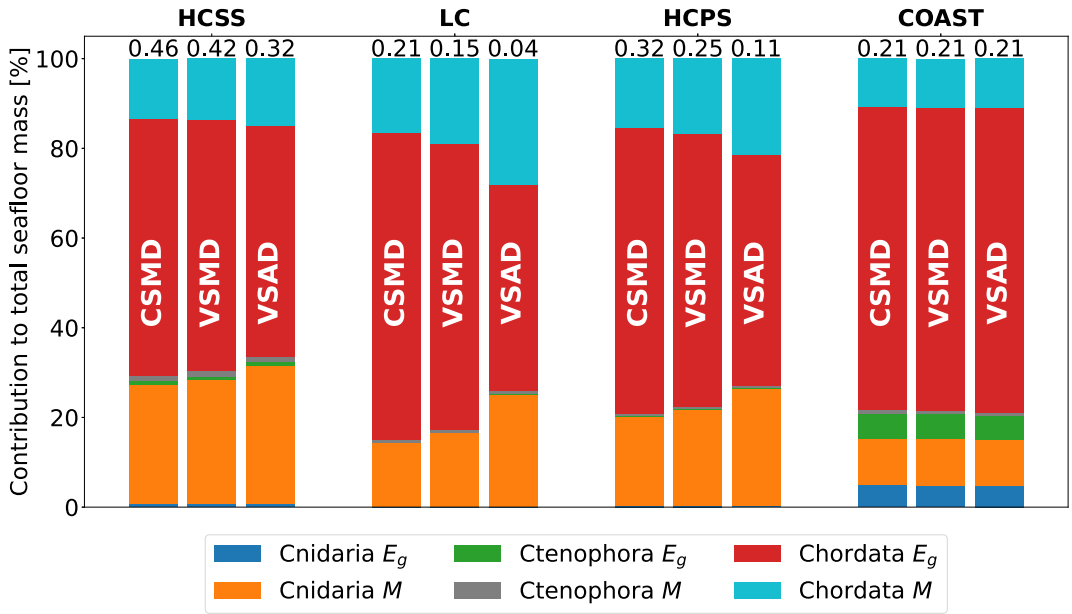

Figure 6. Relative contributions of different GZ-derived particles (egested particles and carcasses) to the total seafloor GZ-POC export in each biome. The first column in each group shows the particle decomposition for a constant sinking speed mass-dependent decay (CSMD). Similarly, the second and third columns show the decomposition for a variable sinking speed mass-(VSMD) and surface area-dependent decay (VSAD), respectively. Dark blue bars correspond to egested Cnidaria particles, orange bars to Cnidaria carcasses, green and red bars to egested Ctenophora and Chordata particles, respectively, whereas gray and light blue bars depict Ctenophora and Chordata carcasses, respectively. The values above each stacked bar correspond to the total GZ-POC export in a given biome for each model in Pg C y^{-1}. HCSS stands for high chlorophyll seasonally stratified, LC for low chlorophyll, HCPS for high chlorophyll permanently stratified and COAST for the coastal biome.

seafloor, where the total global POC export estimate is 2 Pg C y^{-1} (Middelburg, 2019), the differences become more apparent. In the CSMD model, GZ-POC export accounts for 60 % of the total POC export. In the VSMD setup this value is reduced to 52 %, whereas using the VSAD setup, GZ-POC accounts for only 34 % of the total POC export to the seafloor. Nevertheless, this remains a large portion of the total POC export.

The right hand blue axis in Figure 5 shows the GZ POC transfer efficiencies (T_{eff}), that is, the percentage of the total global sum of GZ POC export at either 1000 m or at the seafloor with respect to the total GZ POC export at 100 m. At the depth of 1000 m the transfer efficiency decreases from 47 % (obtained using mass decay and constant sinking speed) to either 44 % (mass decay and variable speed) or even 37 % (surface-area decay and variable speed). Similarly, at the seafloor, transfer efficiencies amount to 31 %, 27 % and 18 % using mass decay with constant sinking speed, mass decay with variable sinking speed and surface-area decay with variable sinking speed, respectively.

3.4. GZ-POC Export per Biome

Next to the initial sinking speed, temperature, through its impact on decay, determines the transfer efficiency of GZ. As it greatly varies between the four biomes, it is of interest to study GZ-POC export in each region separately (Figure 6). In the high chlorophyll seasonally stratified (HCSS) biome (i.e., mid to high latitude ocean), the constant sinking speed mass-dependent decay (CSMD) results in a 0.46 Pg C y^{-1} of GZ-POC export to the ocean floor. In contrast, the variable sinking speed mass-dependent decay (VSMD) export amounts to 0.42 Pg C y^{-1}. Therefore the VSMD setup reduces GZ-POC export by 9 %. Similarly, the export in variable sinking speed surface area-dependent decay (VSAD) of 0.32 Pg C y^{-1} leads to a 30 % reduction in GZ-POC export with respect to the CSMD setup in the HCSS biome.

In the high chlorophyll permanently stratified (HCPS) biome (mostly tropical ocean), these reductions in comparison to the CSMD setup are even more pronounced. Here, the VSMD setup reduces GZ-POC export by 22 %,

while the VSAD setup leads to a 66 % reduction in GZ-POC export. In the coastal ocean (COAST biome) the reduction is insignificant (<1 %) due to shorter sinking times.

Furthermore, notice the importance of initial sinking speed for the transfer efficiency: the relative contribution of the fastest sinking Cnidaria and Chordata carcasses (light blue and orange bars in Figure 6) increases in the VSMD model in comparison to the CSMD setup. This is especially true in the warmer ocean HCPS and low chlorophyll (LC) biomes. In the HCSS biome smaller differences in relative contributions occur, whereas in the coastal biome, they vanish completely.

3.5. Extending Beyond the Current Application

As shown, a coupling between the particle's sinking speed and mass decay, which is dependent on its surface area, greatly decreases export of GZ-POC to the deep sea (Figures 3 and 5). The model equations in this paper were derived for a spherical particle shape, because this allowed for a particularly elegant mathematical formulation of the problem. Specifically, several questionable parameter quantifications were avoided, which had perhaps discouraged previous studies in implementing the model novelties presented here. However, the fact that gelatinous zooplankton exhibit a wide range of morphologies (e.g., oblate medusae, elongated ctenophores, and chain-forming tunicates) does not weaken these novelties. Whatever the particle's shape, its sinking speed must be coupled to its mass decay, that is, equations for sinking and decay must be solved simultaneously and in relation to each other. For non-spherical particles, the full Equation 4 would have to be taken into account. Furthermore, as their size decreases, some particles may shift from the quadratic drag law to the intermediate drag regime (Ploug et al., 2008). Introduction of an intermediate drag regime would increase the drag force at low sinking speeds and likely lead to further reductions in GZ-POC export. This would however require a quantification of several other parameters like the drag coefficient, particle density, characteristic length, and others. Therefore, if a constant sinking speed model is thought of as a zero order model, which works well in cold oceans where decay is slow, the coupling here can be seen as a first order correction term. Further corrections, mentioned above, are of course needed to provide an ever better physical description of particle sinking, which can be built on the mathematics presented in this paper.

In addition, if the particle's decay is a result of a process occurring on its surface, than the modeling should be based on a surface-area-dependent decay. Whatever the particle shape is, a surface area based decay will always lead to a faster decay than a mass dependent decay. Moreover, for a spherical particle, this effect is the weakest of all shapes, because a sphere has the smallest surface-to-volume ratio. Any realistic shape of GZ would therefore lead to a surface-based decay that is faster than a spherical GZ shape. This same reasoning applies to other non-gelatinous particles as well.

This study used initial GZ-POC export production estimates from Luo et al. (2020), to show the effect of the modeling novelties in isolation from other feedback systems. Nevertheless, the VSAD model should be incorporated into fully coupled ecosystem-biogeochemical models that include GZ embedded within plankton food webs, constrained by ambient physical, chemical and biological factors (Clerc et al., 2023; Luo et al., 2022, 2024; Wright et al., 2021). As noted in Clerc et al. (2023), one of the greatest sources of uncertainty is the transfer efficiency, which is among other parameters dependent on the sinking speed. Therefore, the addition of a VSMD or VSAD model should help decrease these uncertainties in future studies. In addition, efforts should be made to more accurately measure sinking speeds of different GZ-POC types, as previously stressed (Tinta et al., 2021).

The precision of models that describe the contributions of gelatinous zooplankton to the biological carbon pump is fundamentally constrained by the scarcity of existing observations. While recent progress has been made with in situ imaging systems (Greer et al., 2023), spatial and temporal coverage remains limited. Global syntheses based on the Jellyfish Database Initiative (Condon et al., 2015; Lucas et al., 2014) and analysis by Lebrato et al. (2019) reveal that gelatinous zooplankton observations are highly uneven and clustered, with vast regions of the ocean lacking any data. Large-scale expeditions such as Tara Oceans have substantially advanced global plankton characterization using combined imaging and molecular approaches, but sampling is limited to fewer than 250 discrete stations worldwide, largely confined to the upper 500 m, and therefore represents only a very small fraction of the ocean volume (Lombard et al., 2024). In contrast, detailed knowledge of gelatinous zooplankton population dynamics and vertical distribution primarily comes from a small number of long-term, regionally focused observatories, notably the MBARI midwater time-series in the northeast Pacific (e.g., Haddock & Choy, 2024; Katija

et al., 2017) and sustained observation programs in Japanese waters (e.g., Lindsay et al., 2008; Lindsay & Hunt, 2005). And yet, these organisms have been recorded in all major oceanic habitats, including mesopelagic and bathypelagic zones, which indicates high adaptability and importance in marine ecosystems, suggesting that a global effort should be made to expand sampling to capture the spatial and temporal variability of these organisms. This would improve current models and provide a better understanding of their role in the biological carbon pump.

4. Conclusions and Future Directions

Constraints on mesopelagic and deep-ocean export remain weak, particularly regarding the fate of rapidly sinking organic particles, which motivates the development of improved representations of these particles. This study presents two novelties in modeling of particulate organic carbon (POC) export into the deep ocean. The first modification consists of replacing the assumption of constant sinking speed with a coupled model, where the change in the decaying particle's mass impacts its sinking speed. The second modification is the introduction of a surface area-dependent mass decay, which reflects the fact that microbial degradation occurs primarily on the surface of the organic particle. Gelatinous zooplankton, proposed as a potentially important, but largely overlooked, contributor to the POC export in the global ocean via its sinking egested particles and carcasses (GZ-POC), were used as a validation case. Results of the model from this study show, that while GZ-POC remains a major contributor to POC export from the euphotic zone, earlier models overestimated GZ-POC contribution to deep-ocean carbon sequestration.

We propose that advancing model representations of sinking organic particles, including variable-speed and surface area-dependent decay schemes, may be key steps toward more accurate modeling of global POC export in the future. The latter is expected to play an important role in models, which incorporate particle fragmentation (e.g., Anderson et al., 2023), where—unlike mass—the total sum of the surface area of fragmented particles increases with time. Fragmentation of GZ carcasses during sinking, particularly during turbulent conditions in the upper mixed layer (as previously reported for different size-range particles in the ocean, Briggs et al., 2020) may strongly alter GZ-POC export, especially for fragile species. Fragmentation (and scavenging) would generate particles of varying sizes, thereby modifying sinking rates, microbial remineralization, and transfer to higher trophic levels or solubilization to dissolved organic matter (Tinta et al., 2021). Hence, efforts should be made to measure fragmentation rates of different types of GZ-particles. In addition, the results from this study revealed the importance of ambient seawater temperature for the fate of organic sinking particles, hence dynamical models should be better constrained by new estimates of temperature dependence of particle decay rates over wider temperature ranges. In the case of GZ-derived particles, sinking speed measurements should be performed for a larger number of GZ species and sizes and along a larger depth range. Above all, the demonstrated transfer efficiency of GZ-derived POC highlights the need for improved characterization of the global GZ spatio-temporal distribution, including the deep sea. Altogether, this study highlights several knowledge gaps that need to be filled to better understand the contribution of gelatinous zooplankton to global POC export and hence the biological carbon pump.

Conflict of Interest

The authors declare no conflicts of interest relevant to this study.

Availability Statement

The coding was done in Python version 3.11.6 inside the OpenDrift environment version 1.11.13 (Dagestad et al., 2018, 2024). Figures were made with Matplotlib version 3.9.2 (Hunter, 2007; The Matplotlib Development Team, 2024). The initial GZ-POC export production values from Luo et al. (2020) were distributed using the python `Shapely` (Gillies et al., 2023) and `Pyproj` (Snow et al., 2019) libraries. The solver code, the remapped bathymetry and remapped ocean temperature data sets, GZ seeding files and CarbonDrift user manual, needed to reproduce the results of this paper, are available under Creative Commons Attribution 4.0 International License at Perharič Bailey (2025).

Acknowledgments
ČEPB, ML, MV and TT were supported by the financial support from the Slovenian Research Agency (research core funding No. P1-0237 and the Slovenian program for young researches). TT would also like to acknowledge funding by Slovenian Research Agency, project number J1-60007. GJH received funding by the FWF, Austria Grant I 4978-B. The authors would like to thank Mario Lebrato for helpful discussions during the making of this study. The authors would like to thank Jessica Luo and other anonymous reviewers together with the editors for their suggestions, which greatly improved this paper.

References

Alcolombri, U., Peaudecerf, F. J., Fernandez, V. I., Behrendt, L., Lee, K. S., & Stocker, R. (2021). Sinking enhances the degradation of organic particles by marine bacteria. *Nature Geoscience*, *14*(10), 775–780. https://doi.org/10.1038/s41561-021-00817-x

Anderson, T. R., Gentleman, W. C., Cael, B. B., Hirschi, J. J.-M., Eastwood, R. L., & Mayor, D. J. (2023). Proliferating particle surface area via microbial decay has profound consequences for remineralisation rate: A new approach to modelling the degradation of sinking detritus in the ocean. *Biogeochemistry*, *164*(2), 335–347. https://doi.org/10.1007/s10533-023-01055-6

Arnosti, C. (2011). Microbial extracellular enzymes and the marine carbon cycle. *Annual Review of Marine Science*, *3*(1), 401–425. https://doi.org/10.1146/annurev-marine-120709-142731

Aumont, O., Ethé, C., Tagliabue, A., Bopp, L., & Gehlen, M. (2015). Pisces-v2: An ocean biogeochemical model for carbon and ecosystem studies. *Geoscientific Model Development*, *8*(8), 2465–2513. https://doi.org/10.5194/gmd-8-2465-2015

Bar-On, Y. M., Phillips, R., & Milo, R. (2018). The biomass distribution on Earth. *Proceedings of the National Academy of Sciences*, *115*(25), 6506–6511. https://doi.org/10.1073/pnas.1711842115

Berzaghi, F., Pinti, J., Aumont, O., Maury, O., Cosimano, T., & Wisz, M. S. (2025). Global distribution, quantification and valuation of the biological carbon pump. *Nature Climate Change*, *15*(4), 385–392. https://doi.org/10.1038/s41558-025-02295-0

Boyd, P., Claustre, H., Levy, M., Siegel, D. A., & Weber, T. (2019). Multi-faceted particle pumps drive carbon sequestration in the ocean. *Nature*, *568*(7752), 327–335. https://doi.org/10.1038/s41586-019-1098-2

Boyd, P., & Trull, T. (2007). Understanding the export of biogenic particles in Oceanic waters: Is there consensus? *Progress in Oceanography*, *72*(4), 276–312. https://doi.org/10.1016/j.pocean.2006.10.007

Boyer, T. P., García, H. E., Locarnini, R. A., Zweng, M. M., Mishonov, A. V., Reagan, J. R., et al. (2018). World ocean atlas 2018 [Dataset]. (Subset used: Temperature) https://www.ncei.noaa.gov/archive/accession/NCEI-WOA18

Briggs, N., Dall'Olmo, G., & Claustre, H. (2020). Major role of particle fragmentation in regulating biological sequestration of CO_2 by the oceans. *Science*, *367*(6479), 791–793. https://doi.org/10.1126/science.aay1790

Buesseler, K. O., Boyd, P. W., Black, E. E., & Siegel, D. A. (2020). Metrics that matter for assessing the ocean biological carbon pump. *Proceedings of the National Academy of Sciences*, *117*(18), 9679–9687. https://doi.org/10.1073/pnas.1918114117

Burd, A. B. (2024). Modeling the vertical flux of organic carbon in the global ocean. *Annual Review of Marine Science*, *16*(16), 135–161. [Journal Article]. https://doi.org/10.1146/annurev-marine-022123-102516

Burd, A. B., Hansell, D. A., Steinberg, D. K., Anderson, T. R., Arístegui, J., Baltar, F., et al. (2010). Assessing the apparent imbalance between geochemical and biochemical indicators of meso- and bathypelagic biological activity: What the @$#! is wrong with present calculations of carbon budgets? *Deep Sea Research Part II: Topical Studies in Oceanography*, *57*(16), 1557–1571. https://doi.org/10.1016/j.dsr2.2010.02.022

Burd, A. B., & Jackson, G. A. (2009). Particle aggregation [Journal Article]. *Annual Review of Marine Science*, *1*(1), 65–90. https://doi.org/10.1146/annurev.marine.010908.163904

Clements, D. J., Yang, S., Weber, T., McDonnell, A. M. P., Kiko, R., Stemmann, L., & Bianchi, D. (2023). New estimate of organic carbon export from optical measurements reveals the role of particle size distribution and export horizon. *Global Biogeochemical Cycles*, *37*(3), e2022GB007633. https://doi.org/10.1029/2022GB007633

Clerc, C., Bopp, L., Benedetti, F., Vogt, M., & Aumont, O. (2023). Including filter-feeding gelatinous macrozooplankton in a global marine biogeochemical model: Model–data comparison and impact on the ocean carbon cycle. *Biogeosciences*, *20*(4), 869–895. https://doi.org/10.5194/bg-20-869-2023

Condon, R. H., Lucas, C. H., Duarte, C. M., & Pitt, K. A. (2015). JeDI: The jellyfish database initiative. *National Center for Ecological Analysis and Synthesis (NCEAS)*. https://doi.org/10.1575/1912/7191

Dagestad, K.-F., Röhrs, J., Breivik, Ø., & Aadlandsvik, B. (2024). Openddrift, an open source framework for ocean trajectory modelling [Software]. Retrieved from https://opendrift.github.io/history_link.html#release-v1-11-13

Dagestad, K.-F., Röhrs, J., Breivik, Ø., & Ådlandsvik, B. (2018). Opendrift v1.0: A generic framework for trajectory modelling. *Geoscientific Model Development*, *11*(4), 1405–1420. https://doi.org/10.5194/gmd-11-1405-2018

de Boyer Montégut, C. (2023). Mixed layer depth climatology computed with a density threshold criterion of 0.03kg/m^3 from 10 m depth value [Dataset]. *SEANOE*. https://doi.org/10.17882/91774

de Boyer Montégut, C., Madec, G., Fischer, A. S., Lazar, A., & Iudicone, D. (2004). Mixed layer depth over the global ocean: An examination of profile data and a profile-based climatology. *Journal of Geophysical Research*, *109*(C12). https://doi.org/10.1029/2004JC002378

DeVries, T., & Weber, T. (2017). The export and fate of organic matter in the ocean: New constraints from combining satellite and oceanographic tracer observations. *Global Biogeochemical Cycles*, *31*(3), 535–555. https://doi.org/10.1002/2016GB005551

Enke, T. N., Leventhal, G. E., Metzger, M., Saavedra, J. T., & Cordero, O. X. (2018). Microscale ecology regulates particulate organic matter turnover in model marine microbial communities. *Nature Communications*, *9*(1), 2743. https://doi.org/10.1038/s41467-018-05159-8

E.U. Copernicus Marine Service (CMEMS). (2023). Global ocean physics reanalysis [Dataset]. https://doi.org/10.48670/moi-00021

Fadeev, E., Hennenfeind, J. H., Amano, C., Zhao, Z., Klun, K., Herndl, G. J., & Tinta, T. (2024). Bacterial degradation of ctenophore *Mnemiopsis leidyi* organic matter. *mSystems*, *9*(2), e01264-23. https://doi.org/10.1128/msystems.01264-23

Field, C. B., Behrenfeld, M. J., Randerson, J. T., & Falkowski, P. (1998). Primary production of the biosphere: Integrating terrestrial and Oceanic components. *Science*, *281*(5374), 237–240. https://doi.org/10.1126/science.281.5374.237

Giering, S. L. C., & Evans, C. (2022). Overestimation of prokaryotic production by leucine Incorporation—And how to avoid it. *Limnology & Oceanography*, *67*(3), 726–738. https://doi.org/10.1002/lno.12032

Gillies, S., van der Wel, C., Van den Bossche, J., Taves, M. W., Arnott, J., Ward, B. C., et al. (2023). Shapely: Manipulation and analysis of geometric objects [Software]. *Zenodo*. https://doi.org/10.5281/zenodo.7583915

Greer, A. T., Schmid, M. S., Duffy, P. I., Robinson, K. L., Genung, M. A., Luo, J. Y., et al. (2023). In situ imaging across ecosystems to resolve the fine-scale oceanographic drivers of a globally significant planktonic grazer. *Limnology & Oceanography*, *68*(1), 192–207. https://doi.org/10.1002/lno.12259

Guy-Haim, T., Rubin-Blum, M., Rahav, E., Belkin, N., Silverman, J., & Sisma-Ventura, G. (2020). The effects of decomposing invasive jellyfish on biogeochemical fluxes and microbial dynamics in an ultra-oligotrophic sea. *Biogeosciences*, *17*(22), 5489–5511. https://doi.org/10.5194/bg-17-5489-2020

Haddock, S. H., & Choy, C. A. (2024). Life in the midwater: The ecology of deep pelagic animals. *Annual Review of Marine Science*, *16*(1), 383–416. [Journal Article]. https://doi.org/10.1146/annurev-marine-031623-095435

Henson, S. A., Sanders, R., & Madsen, E. (2012). Global patterns in efficiency of particulate organic carbon export and transfer to the deep ocean. *Global Biogeochemical Cycles*, *26*(1). https://doi.org/10.1029/2011gb004099

Henson, S. A., Sanders, R., Madsen, E., Morris, P. J., Le Moigne, F., & Quartly, G. D. (2011). A reduced estimate of the strength of the ocean's biological carbon pump. *Geophysical Research Letters*, *38*(4). https://doi.org/10.1029/2011GL046735

Herndl, G. J., Bayer, B., Baltar, F., & Reinthaler, T. (2023). Prokaryotic life in the deep Ocean's water column [Journal Article]. *Annual Review of Marine Science*, *15*(15), 461–483. https://doi.org/10.1146/annurev-marine-032122-115655

Herndl, G. J., & Reinthaler, T. (2013). Microbial control of the dark end of the biological pump. *Nature Geoscience*, *6*(9), 718–724. https://doi.org/10.1038/ngeo1921

Hunter, J. D. (2007). Matplotlib: A 2d graphics environment. *Computing in Science & Engineering*, *9*(3), 90–95. https://doi.org/10.1109/MCSE.2007.55

Iversen, M. H. (2023). Carbon export in the ocean: A biologist's perspective. *Annual Review of Marine Science*, *15*(1), 357–381. https://doi.org/10.1146/annurev-marine-032122-035153

Johnson, W. M., Longnecker, K., Kido Soule, M. C., Arnold, W. A., Bhatia, M. P., Hallam, S. J., et al. (2020). Metabolite composition of sinking particles differs from surface suspended particles across a latitudinal transect in the south Atlantic. *Limnology & Oceanography*, *65*(1), 111–127. https://doi.org/10.1002/lno.11255

Katija, K., Sherlock, R. E., Sherman, A. D., & Robison, B. H. (2017). New technology reveals the role of giant Larvaceans in Oceanic carbon cycling. *Science Advances*, *3*(5), e1602374. https://doi.org/10.1126/sciadv.1602374

Kriest, I., & Oschlies, A. (2015). Mops-1.0: Towards a model for the regulation of the global oceanic nitrogen budget by marine biogeochemical processes. *Geoscientific Model Development*, *8*(9), 2929–2957. https://doi.org/10.5194/gmd-8-2929-2015

Lebrato, M., Molinero, J.-C., Cartes, J., Lloris, D., Mélin, F., & Beni-Casadella, L. (2013). Sinking jelly-carbon unveils potential environmental variability along a continental margin. *PLoS One*, *8*(12), e82070. https://doi.org/10.1371/journal.pone.0082070

Lebrato, M., Pahlow, M., Frost, J. R., Küter, M., de Jesus Mendes, P., Molinero, J.-C., & Oschlies, A. (2019). Sinking of gelatinous zooplankton biomass increases deep carbon transfer efficiency globally. *Global Biogeochemical Cycles*, *33*(12), 1764–1783. https://doi.org/10.1029/2019GB006265

Lebrato, M., Pahlow, M., Oschlies, A., Pitt, K. A., Jones, D. O. B., Molinero, J. C., & Condon, R. H. (2011). Depth attenuation of organic matter export associated with jelly falls. *Limnology & Oceanography*, *56*(5), 1917–1928. https://doi.org/10.4319/lo.2011.56.5.1917

Lebrato, M., Pitt, K., Sweetman, A., Jones, D., Cartes, J., Oschlies, A., et al. (2012). Jelly-falls historic and recent observations: A review to drive future research direction. *Hydrobiologia*, *690*(1), 227–245. https://doi.org/10.1007/s10750-012-1046-8

Le Quéré, C., Andrew, R. M., Friedlingstein, P., Sitch, S., Hauck, J., Pongratz, J., et al. (2018). Global carbon budget 2018. *Earth System Science Data*, *10*(4), 2141–2194. https://doi.org/10.5194/essd-10-2141-2018

Lindsay, D. J., & Hunt, J. C. (2005). Biodiversity in midwater cnidarians and ctenophores: Submersible-based results from deep-water bays in the Japan Sea and north-western Pacific. *Journal of the Marine Biological Association of the United Kingdom*, *85*(3), 503–517. https://doi.org/10.1017/S0025315405011434

Lindsay, D. J., Pagès, F., Corbera, J., Miyake, H., Hunt, J. C., Ichikawa, T., et al. (2008). The anthomedusan fauna of the Japan trench: Preliminary results from in situ surveys with manned and unmanned vehicles. *Journal of the Marine Biological Association of the United Kingdom*, *88*(8), 1519–1539. https://doi.org/10.1017/S0025315408002051

Locarnini, R. A., Mishonov, A. V., Baranova, O. K., Boyer, T. P., Zweng, M. M., Garcia, H. E., et al. (2018). *World ocean atlas 2018, volume 1: Temperature (Report)*. NOAA Atlas NESDIS 81. Retrieved from https://archimer.ifremer.fr/doc/00651/76338/

Lombard, F., Guidi, L., Brandão, M. C., Coelho Luis, P., Colin, S., Dolan, R. J., et al. (2024). Ubiquity of inverted "gelatinous" ecosystem pyramids in the global ocean. *bioRxiv*. https://doi.org/10.1101/2024.02.09.579612

Lucas, C. H., Jones, D. O., Hollyhead, C. J., Condon, R. H., Duarte, C. M., Graham, W. M., et al. (2014). Gelatinous zooplankton biomass in the global oceans: Geographic variation and environmental drivers. *Global Ecology and Biogeography*, *23*(7), 701–714. https://doi.org/10.1111/geb.12169

Luo, J. Y., Condon, R. H., Stock, C. A., Duarte, C. M., Lucas, C. H., Pitt, K. A., & Cowen, R. K. (2020). Gelatinous zooplankton-mediated carbon flows in the global oceans: A data-driven modeling study. *Global Biogeochemical Cycles*, *34*(9), e2020GB006704. https://doi.org/10.1029/2020GB006704

Luo, J. Y., Stock, C. A., Dunne, J. P., Saba, G. K., & Cook, L. (2024). Ocean biogeochemical fingerprints of fast-sinking tunicate and fish detritus. *Geophysical Research Letters*, *51*(3), e2023GL107052. https://doi.org/10.1029/2023GL107052

Luo, J. Y., Stock, C. A., Henschke, N., Dunne, J. P., & O'Brien, T. D. (2022). Global ecological and biogeochemical impacts of pelagic tunicates. *Progress in Oceanography*, *205*, 102822. https://doi.org/10.1016/j.pocean.2022.102822

Martin, J. H., Knauer, G. A., Karl, D. M., & Broenkow, W. W. (1987). Vertex: Carbon cycling in the northeast pacific. *Deep-Sea Research, Part A: Oceanographic Research Papers*, *34*(2), 267–285. https://doi.org/10.1016/0198-0149(87)90086-0

Middelburg, J. J. (2019). *Marine carbon biogeochemistry: A primer for Earth system scientists*. Springer Nature.

NASA Ocean Biology Processing Group. (2025). Sea-viewing wide field-of-view sensor (seawifs) level-3 mapped ocean color data [Dataset]. *NASA Ocean Biology Distributed Active Archive Center*. Retrieved from https://oceandata.sci.gsfc.nasa.gov/directdataaccess/Level-3%20Mapped/SeaWiFS/

Nguyen, T. T. H., Zakem, E. J., Ebrahimi, A., Schwartzman, J., Caglar, T., Amarnath, K., et al. (2022). Microbes contribute to setting the ocean carbon flux by altering the fate of sinking particulates. *Nature Communications*, *13*(1), 1657. https://doi.org/10.1038/s41467-022-29297-2

NOAA National Centers for Environmental Information. (2022). Etopo 2022 15 arc-second global relief model [Dataset]. *NOAA national centers for environmental information*. https://doi.org/10.25921/fd45-gt74

Nowicki, M., DeVries, T., & Siegel, D. A. (2022). Quantifying the carbon export and sequestration pathways of the ocean's biological carbon pump. *Global Biogeochemical Cycles*, *36*(3), e2021GB007083. https://doi.org/10.1029/2021GB007083

Omand, M. M., Govindarajan, R., He, J., & Mahadevan, A. (2020). Sinking flux of particulate organic matter in the oceans: Sensitivity to particle characteristics. *Scientific Reports*, *10*(1), 5582. https://doi.org/10.1038/s41598-020-60424-5

Perharič Bailey, C. E. (2025). Carbondrift: First release [Software]. *Zenodo*. https://doi.org/10.5281/zenodo.15387011

Ploug, H., Iversen, M. H., & Fischer, G. (2008). Ballast, sinking velocity, and apparent diffusivity within marine snow and zooplankton fecal pellets: Implications for substrate turnover by attached bacteria. *Limnology and Oceanography*, *53*(5), 1878–1886. https://doi.org/10.4319/lo.2008.53.5.1878

Schulzweida, U. (2023). Cdo user guide [Software]. *Zenodo*. https://doi.org/10.5281/zenodo.10020800

Siegel, D. A., Buesseler, K. O., Doney, S. C., Sailley, S. F., Behrenfeld, M. J., & Boyd, P. W. (2014). Global assessment of ocean carbon export by combining satellite observations and food-web models. *Global Biogeochemical Cycles*, *28*(3), 181–196. https://doi.org/10.1002/2013GB004743

Snow, A. D., Whitaker, J., Cochran, M., Miara, I., Van den Bossche, J., Mayo, C., et al. (2019). Pyproj, cartographic projections and coordinate transformations library [Software]. *Zenodo*. https://doi.org/10.5281/zenodo.7776548

Steinberg, D. K., & Landry, M. R. (2017). Zooplankton and the ocean carbon cycle. *Annual Review of Marine Science*, *9*(1), 413–444. https://doi.org/10.1146/annurev-marine-010814-015924

Stukel, M. R., & Ducklow, H. W. (2017). Stirring up the biological pump: Vertical mixing and carbon export in the Southern Ocean. *Global Biogeochemical Cycles*, *31*(9), 1420–1434. https://doi.org/10.1002/2017GB005652

Sweetman, A. K., Chelsky, A., Pitt, K. A., Andrade, H., van Oevelen, D., & Renaud, P. E. (2016). Jellyfish decomposition at the seafloor rapidly alters biogeochemical cycling and carbon flow through benthic food-webs. *Limnology & Oceanography*, *61*(4), 1449–1461. https://doi.org/10.1002/lno.10310

Sweetman, A. K., Smith, C. R., Dale, T., & Jones, D. O. (2014). Rapid scavenging of jellyfish carcasses reveals the importance of gelatinous material to deep-sea food webs. *Proceedings of the Royal Society B: Biological Sciences*, *281*(1796), 20142210. https://doi.org/10.1098/rspb.2014.2210

The Matplotlib Development Team. (2024). Matplotlib: Visualization with python [Software]. *Zenodo*. https://doi.org/10.5281/zenodo.13308876

Tinta, T., Klun, K., & Herndl, G. J. (2021). The importance of jellyfish–microbe interactions for biogeochemical cycles in the ocean. *Limnology & Oceanography*, *66*(5), 2011–2032. https://doi.org/10.1002/lno.11741

Tinta, T., Zhao, Z., Bayer, B., & Herndl, G. J. (2023). Jellyfish detritus supports niche partitioning and metabolic interactions among pelagic marine bacteria. *Microbiome*, *11*(1), 156. https://doi.org/10.1186/s40168-023-01598-8

Tinta, T., Zhao, Z., Escobar, A., Klun, K., Bayer, B., Amano, C., et al. (2020). Microbial processing of jellyfish detritus in the ocean. *Frontiers in Microbiology*, *11*, 590995. https://doi.org/10.3389/fmicb.2020.590995

Turner, J. T. (2015). Zooplankton fecal pellets, marine snow, phytodetritus and the ocean's biological pump. *Progress in Oceanography*, *130*, 205–248. https://doi.org/10.1016/j.pocean.2014.08.005

Wright, R. M., Le Quéré, C., Buitenhuis, E., Pitois, S., & Gibbons, M. J. (2021). Role of jellyfish in the plankton ecosystem revealed using a global ocean biogeochemical model. *Biogeosciences*, *18*(4), 1291–1320. https://doi.org/10.5194/bg-18-1291-2021

Yool, A., Popova, E. E., & Anderson, T. R. (2013). Medusa-2.0: An intermediate complexity biogeochemical model of the marine carbon cycle for climate change and ocean acidification studies. *Geoscientific Model Development*, *6*(5), 1767–1811. https://doi.org/10.5194/gmd-6-1767-2013